Experimental Verification of Impedance Matching Method for Repeater to Improve Spatial Freedom of 6.78 MHz Resonant Inductive Coupling Wireless Power Transfer Systems

Keita Fujiki, Masataka Ishihara, Kazuhiro Umetani, Eiji Hiraki
Graduate School of Natural Science and Technology
Okayama University
Okayama, Japan

Published in: 2019 21st European Conference on Power Electronics and Applications (EPE'19 ECCE Europe)

DOI: 10.23919/EPE.2019.8915171

Experimental Verification of Impedance Matching Method for Repeater to Improve Spatial Freedom of 6.78 MHz Resonant Inductive Coupling Wireless Power Transfer Systems

Keita Fujiki, Masataka Ishihara, Kazuhiro Umetani, Eiji Hiraki
OKAYAMA UNIVERSITY / 3-1-1 Tsushimanaka, Kita-ku
Okayama, Japan
Tel.: +81/(86)–2518115
Fax: +81/(86)–2518256
E-Mail: pu861z88@s.okayama-u.ac.jp

Keywords

«Wireless power transmission», «Contactless Energy Transfer», «Gallium Nitride (GaN)»

Abstract

Placing a repeater, which relays the magnetic field from the transmitter to the receiver, is promising as a method to increase the spatial freedom of resonant inductive coupling wireless power transfer systems (RIC-WPT) working at 6.78MHz. However, the capability of the repeater is often affected by a frequency splitting phenomenon. When this phenomenon occurs, the resonance in the repeater becomes sufficiently small at a fixed operating frequency and make it difficult to improve the spatial freedom. To solve this problem, we apply an impedance matching method using simple switching circuits to the 6.78 RIC-WPT system with the repeater. Then we carry out experiments to verify the effectiveness of the impedance matching method. The experimental results show that the repeater improves the spatial freedom of the 6.78 MHz RIC-WPT regardless of the frequency splitting phenomenon.

Introduction

Recently, wireless power transfer (WPT) techniques are attracting public attention because of their convenience and safety. In particular, resonant inductive coupling WPT (RIC-WPT) systems working at kHz to MHz are expected to be applied to various applications because the RIC-WPT systems achieve comparatively the high efficiency and high output power. Usually, to obtain the high output power, the strong magnetic coupling is needed because the RIC-WPT systems transfer the power via magnetically coupled coils. However, in the case of the low-power applications such as home appliances [1], mobile devices [2] and biomedical devices [3], gaining enough strong magnetic coupling is often difficult because the size of the receiver coil is limited due to an allowed installing area. Hence, the spatial freedom of the WPT for the low power applications tend to be low, which impairs the convenience [4].

As an approach to improve the spatial freedom, the RIC-WPT system working at MHz is effective compared with the RIC-WPT systems working at kHz. A higher operating frequency helps to increase output power [5]. Among the MHz RIC-WPT systems, the RIC-WPT systems working at 6.78 ±0.015 MHz (the lowest frequency of Industrial Scientific Medical (ISM) band) are widely studied [5-7].

As another method to further increase the spatial freedom, placing a repeater is also widely studied [8-10]. Figure 1 shows the RIC-WPT system with the repeater, where W_1, W_2, and W_3 are the transmitting, repeating, and receiving coils, respectively. The repeater is an LC resonator composed of only a coil and a capacitor, and its resonant frequency is designed to be equal to the resonant frequency of the transmitter and receiver. The repeater can be placed in an arbitrary position because the repeater is physically independent of the transmitter and receiver. The repeater relays the magnetic field from the transmitter to the receiver. The resonance in the repeater is easily excited even by a weak magnetic field from the transmitter because the repeater usually has a high quality-factor (Q-factor). The repeater current by this resonance generates the magnetic field around the repeater, which transfers the power to the receiver. Therefore, to relay the magnetic field from the transmitter to the receiver effectively, a

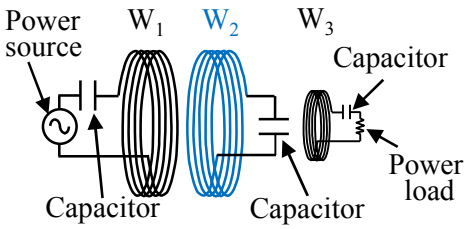

Fig. 1: RIC-WPT system with repeater

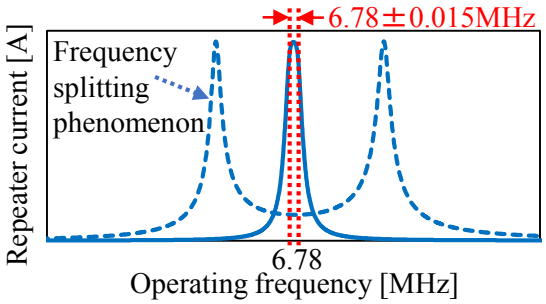

Fig. 2: Influence of frequency splitting phenomenon

large repeater current is important [8]. As a result, the receiver located relatively far from the power transmitter can receive the sufficient power. Based on the above considerations, adding the repeater to the 6.78MHz RIC-WPT system is an effective approach to increase the spatial freedom.

Despite these attractive advantages, the repeater is not practical due to a frequency splitting phenomenon [9-13]. The repeater often suffers from the frequency splitting phenomenon because of its high Q-factor. When the frequency splitting phenomenon occurs, the frequency for maximizing the repeater current (i.e., the initially designed resonant frequency) is split into several different frequencies as shown in Fig. 2, and to excite the resonance in the repeater becomes difficult at the initially designed resonant frequency. Accordingly, a large repeater current may not be obtained in the narrow frequency range of 6.78 ±0.015 MHz when the frequency splitting phenomenon occurs. Therefore, the resonant frequency of the resonators must be adjusted so that one of the frequencies corresponding to the peaks is equal to the operating frequency within the range of 6.78 ±0.015 MHz [7]. However, the frequencies corresponding to the peaks shift according to the coupling coefficient between the repeating coil and the other coil [9-13]. Hence, the resonant frequency of the resonators must be adjusted accurately according to the location of the repeater. Consequently, in practice, the repeater placed in an arbitrary position cannot increase the spatial freedom.

To address this problem, as for the kHz RIC-WPT system, the previous study [14] proposed an impedance matching method for maximizing the repeater current. The previous study [14] applied a simple switching circuit named Automatic Tuning Assist Circuit (ATAC) to the transmitter and the repeater. The previous study [14] revealed that the ATACs realize a constant large repeater current regardless of the frequency splitting phenomenon. This method is attractive because the troublesome adjustments of the resonant frequencies are replaced with slight control of the ATAC on the repeater. Therefore, this method may realize the practical repeater which improves the spatial freedom even if it is placed in an arbitrary position.

However, it is not clear whether the impedance matching method using the ATACs are also effective for the practical 6.78 MHz RIC-WPT systems to improve the spatial freedom. The previous study [14] only focused on maximizing the repeater current, and the discussion of [14] was limited to the system without the receiver. In other words, the contribution to the spatial freedom improvement of the receiver by maximizing the repeater current is not clear. Therefore, it is necessary to expand the discussion to the system including the receiver to investigate the improvement of the spatial freedom. Furthermore, the experiments in [14] were carried out at about 100 kHz. In this case, [14] pointed out that the Q-factor of the resonators equivalently decreased due to a slight loss of the ATACs. However, the loss of the ATACs may further increase at 6.78 MHz.

Therefore, the purpose of this study is to reveal that the impedance matching method using the ATACs is effective for improving the spatial freedom of the 6.78 MHz RIC-WPT systems. For this purpose, we carry out the analysis including the receiver and show that the repeater current can be maximized even if there is the receiver. Then, for the experiments, we construct the 6.78 MHz RIC-WPT system with the ATACs. The experimental results show that the impedance matching method using the ATACs can improve the spatial freedom of the 6.78 MHz RIC-WPT system regardless of the frequency splitting phenomenon even if the repeater is placed in an arbitrary position.

Review of Impedance Matching Method Using ATACs

This section reviews the impedance matching method for the repeater using the ATACs. For this purpose, first subsection reviews the operating principle of the ATAC.

Operating Principle of ATAC

The ATAC was originally proposed to achieve a unity power factor of the power source connected to the transmitter [15]. Figure 3 shows the transmitter with the ATAC, where V_{IN} is the voltage of the power source, I_1 is the transmitter current, V_{ATAC} is the output voltage of the ATAC, r_1 is the parasitic resistance of W_1, L_1 is the self-inductance of W_1, and C_1 is the capacitance of the resonance capacitor. The ATAC consists of only the switches and the decoupling capacitor. The DC bus of the ATAC does not have any additional DC voltage source.

The ATAC operates as to cancel a voltage drop of the reactance in the transmitter automatically. Fig. 4 shows the key waveforms of Fig. 3. As shown in Fig. 4, the ATAC operates with the fixed constant phase difference of $\pi/2$ from V_{IN}. The ATAC does not have ideally any resistive components. Therefore, in the steady state, the ATAC does not receive the active power, which means that the phase difference between V_{ATAC} and I_1 must always be $\pi/2$. The amplitude of V_{ATAC} is automatically determined so that the phase difference between V_{ATAC} and I_1 is $\pi/2$. Consequently, the ATAC can achieve unity power factor of the power source by only setting the phase difference between V_{IN} and V_{ATAC} to $\pi/2$ regardless of the operating frequency [15]. Based on this operation, in the equivalent circuit (See Fig. 5), the ATAC can be expressed as the AC voltage source, where V_{A1} is the voltage of the ATAC.

Impedance Matching Method Using ATACs for Maximizing Repeater Current

Then, this subsection reviews the RIC-WPT with the impedance matching method for maximizing repeater current using the ATACs. Figure 6 shows the equivalent circuit. The ATAC is applied to the transmitter and the repeater. The circuit configuration of the transmitting side is same as Fig. 3. In [14], the receiver was ignored because it was assumed that the receiver receives only very small power. Symbol r_2 is the parasitic resistance of W_2; L_2 is the self-inductance of W_2; M_{12} is the mutual inductance between W_1 and W_2; C_2 is the capacitance of the resonance capacitor; V_{A2} is the voltage of the ATAC

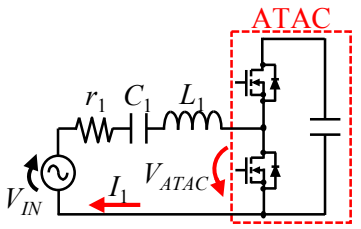

Fig. 3: Transmitter with ATAC

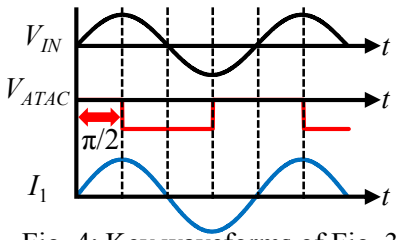

Fig. 4: Key waveforms of Fig. 3

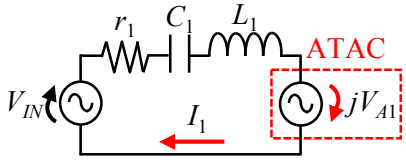

Fig. 5: Equivalent circuit of Fig. 3

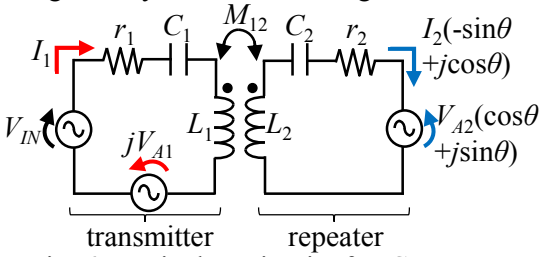

Fig. 6: Equivalent circuit of RIC-WPT proposed in previous study

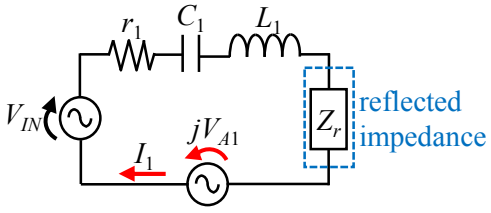

Fig. 7: Equivalent circuit with reflected impedance of Fig. 6

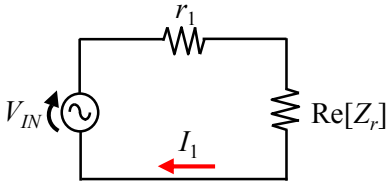

Fig. 8: Equivalent circuit of Fig. 7 based on operating principle of ATAC

on the repeating side; I_2 is the repeater current. As shown in Fig. 6, the ATAC on the repeating side operates with the variable phase difference θ from V_{IN}. The phase difference of θ is controlled to maximize I_2.

The phase difference θ has an optimum value θ_{opt} for maximizing I_2. Figure 7 shows the equivalent circuit based on a reflected impedance Z_r [16-17]. The repeating side is modeled as the reflected impedance Z_r on the transmitting side, where Z_r can be expressed as

$$Z_r = (\omega M_{12}\cos\theta)^2 / r_2 + j\omega^2 M_{12}^2 \sin\theta\cos\theta / r_2 . \tag{1}$$

Based on the operating principle of the ATAC, the all reactance of Fig. 7 can be canceled by the ATAC on the transmitting side. As a result, Fig. 7 can be transformed as Fig. 8. To maximize I_2, it is necessary to maximize the power consumption on the repeating side. In other words, the power consumption of the real part of Z_r must be maximized. Consequently, θ_{opt} and I_2 at θ_{opt} can be derived as

$$\theta_{opt} = \pm\cos^{-1}\left(1/k_{12}\sqrt{Q_1 Q_2}\right), \quad I_2|_{\theta=\theta_{opt}} = V_{IN}/2\sqrt{r_1 r_2}, \tag{2}$$

where k_{12} is the coupling coefficient, i.e. $k_{12}=M_{12}/(L_1L_2)^{1/2}$, Q_1 and Q_2 are the Q-factor of the transmitter and the repeater, respectively, i.e. $Q_1=\omega L_1/r_1$ and $Q_2=\omega L_2/r_2$. From (2), I_2 can be maximized to the constant value regardless of the operating frequency and the coupling coefficient. The above is the operating principle of the impedance matching method using the ATACs.

Analysis Considering Receiver

The purpose of this section is to reveal that the repeater current can be maximized even in the system considering the receiver by adjusting the phase difference of the ATAC on the repeating side. For this purpose, we derive the optimum phase difference θ_{opt}' for maximizing the repeater current.

Figure 9 shows the equivalent circuit of the RIC-WPT with the ATACs considering the receiver, where r_3 is the parasitic resistance of W_3, L_3 is the self-inductance of W_3, C_3 is the capacitance of the resonance capacitor, R_o is the equivalent AC resistance of the load resistance including the rectifier[16-17], and I_3 is the receiver current. M_{23} and M_{31} are the mutual inductances between each coil, where the coupling coefficients are defined as $k_{23}=M_{23}/(L_2L_3)^{1/2}$ and $k_{31}=M_{31}/(L_3L_1)^{1/2}$. First, we model the receiver

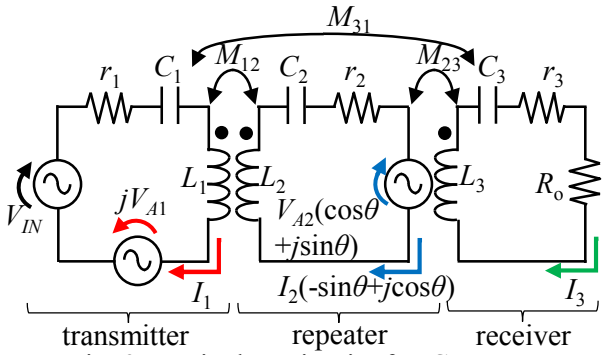

Fig. 9: Equivalent circuit of RIC-WPT with ATACs considering receiver

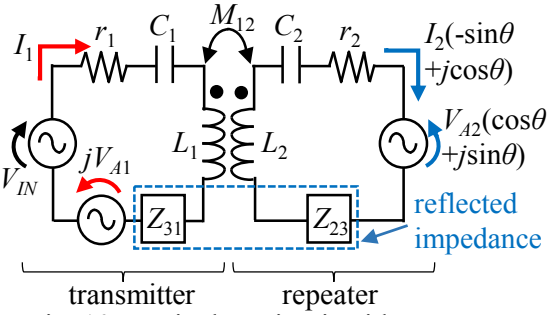

Fig. 10: Equivalent circuit with reflected impedance of Fig. 9

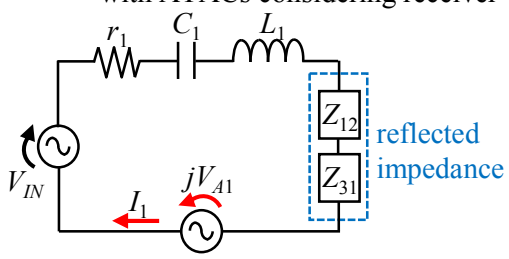

Fig. 11: Equivalent circuit with reflected impedance of Fig. 10

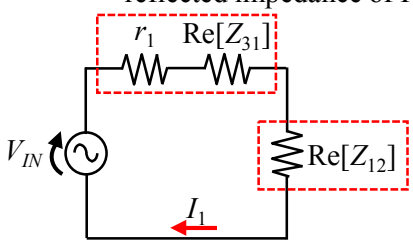

Fig. 12: Equivalent circuit of Fig. 11 based on operating principle of ATAC

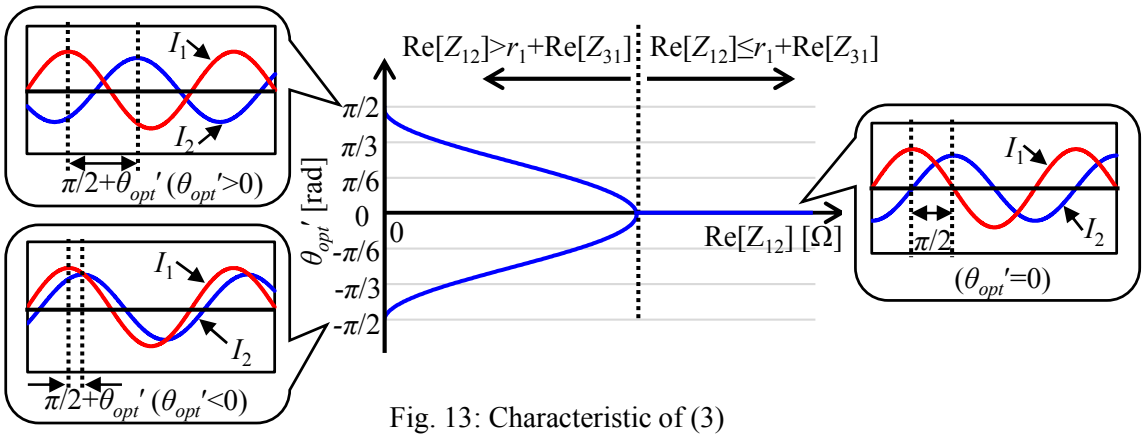

Fig. 13: Characteristic of (3)

as the reflected impedance (Z_{31} and Z_{23}) of the transmitter and repeater. Hence, we obtain Fig. 10. Then, we model the repeater including Z_{23} as the reflected impedance Z_{12} of the transmitter. As a result, we obtain Fig. 11. Based on the operating principle of the ATAC, the ATAC on the transmitting side cancels not only the reactance of L_1 and C_1 but also the imaginary parts of Z_{12} and Z_{31}. Consequently, we obtain the final equivalent circuit of Fig. 12. The impedance of Z_{12} can be adjusted by θ.

To maximize the repeater current, we have to maximize the power consumption of Re[Z_{12}] in Fig. 12. Therefore, we need to adjust θ to satisfy Re[Z_{12}]=r_1+Re[Z_{31}]. Then, for the simplicity of the analysis, we introduce the following two approximations.

1. The reactance of the receiver is adjusted to be zero at the operating frequency, i.e., $\omega L_3 - 1/\omega C_3 \approx 0$.
2. $k_{12}^2 >> k_{23}^2 k_{31}^2 Q_3^2$.

In the second approximation, Q_3 is the Q-factor of the receiver, i.e., $Q_3=\omega L_3/(r_3+R_o)$. The first approximation is reasonable when an active rectifier is applied to the receiver. In this paper, we assume that the active rectifier is applied to the receiver. The active rectifier equivalently cancels the voltage drop of the reactance in the receiver [6]. Then, the second approximation is reasonable in the case of low power applications. The size of the receiver tends to be smaller than the sizes of the transmitter and repeater. Hence, k_{23}^2 and k_{31}^2 are usually smaller than k_{12}^2. Furthermore, Q_3 is comparatively small because Q_3 includes the load resistance. Based on the above considerations, two approximations are reasonable for deriving θ_{opt}'. Consequently, θ for maximizing the repeater current can be derived as

$$\theta_{opt}' \approx \begin{cases} \pm\cos^{-1}\left(\sqrt{(1+k_{23}^2 Q_2 Q_3 + k_{31}^2 Q_3 Q_1)/k_{12}^2 Q_1 Q_2}\right) & \left(\mathrm{Re}[Z_{12}] > r_1 + \mathrm{Re}[Z_{31}]\right), \\ 0 & \left(\mathrm{Re}[Z_{12}] \le r_1 + \mathrm{Re}[Z_{31}]\right). \end{cases} \tag{3}$$

Figure 13 shows the characteristic of (3). In the case of Re[Z_{12}]≤r_1+Re[Z_{31}], there is one solution of θ_{opt}', and θ_{opt}'=0. Based on the operating principle of the ATAC, the phase difference between I_1 and I_2 is π/2. Then, in the case of Re[Z_{12}]>r_1+Re[Z_{31}], there are two solutions of θ_{opt}' according to the positive or negative signs. As shown in Fig. 13, when the sign of θ_{opt}' is set to negative, the phase of I_2 approaches the same phase of I_1. On the other hand, when the sign of θ_{opt}' is set to positive, the phase of I_2 approaches the opposite phase of I_1. As pointed out in [11], the magnetic field generated by two resonators depends on the phase difference between the currents in the resonators. Therefore, an appropriate sign of θ_{opt}' must be selected according to the position of the receiver in the case of Re[Z_{12}]>r_1+Re[Z_{31}].

Experimental Verification

The purpose of this section is to verify the effectiveness of the impedance matching method using the ATACs for improving the spatial freedom of the 6.78 MHz RIC-WPT systems. For this purpose, in this section, first, we construct the 6.78 MHz RIC-WPT system with the ATACs. Then, we describe the experimental setup. Finally, we show the experimental results.

Circuit Configuration

This subsection describes the circuit configuration for the experiments. Figure 14 shows the circuit configuration. As shown in Fig. 14, the power source connected to the transmitter consists of the DC voltage source and the half-bridge inverter.

In this study, GaN FETs manufactured by Efficient Power Conversion Corporation (EPC), Inc. are adopted as the switches of the half-bridge inverter and the ATACs. To ensure the high spatial freedom, lowering of the *Q*-factors due to the loss of the ATACs must be suppressed. The GaN FET is known as a promising switch to achieve low on-resistance and fast switching capability simultaneously. This attractive feature helps to prevent lowering of the *Q*-factors. In spite of this advantage, the GaN FET is susceptible to false triggering such as self-turn-on due to the parasitic inductance of the wiring [18-19]. Therefore, the PCB design to suppress the parasitic inductance is quite important. In this study, based on [19], we designed the PCB to prevent the false triggering.

In this study, driving signals for the ATACs on the transmitting and repeating sides are generated by using a synchronized signal generator. Furthermore, for power supplies for gate drivers of the ATACs, an external power source is used. Hence, the ATAC on the repeating side connected to the ATAC on the transmitting side by wiring via the synchronized signal generator and the external power supply. Certainly, although the advantage of the repeater is that it is physically independent of the transmitter, self-drive i.e., driving the ATAC on the repeating side without the synchronized signal

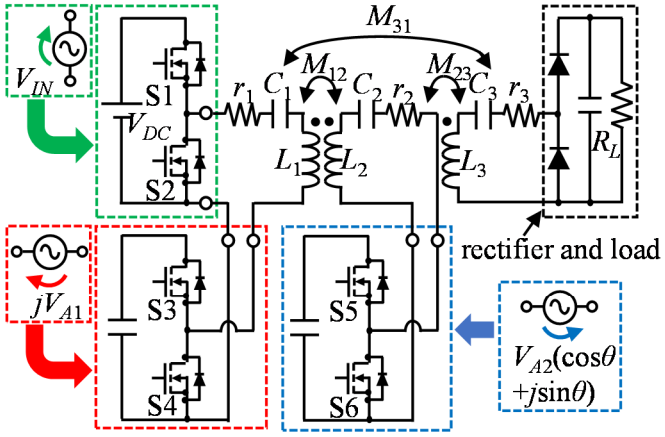

Fig. 14: Circuit configuration of experimental verification

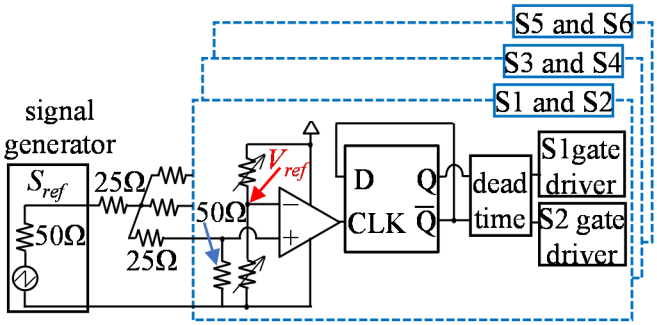

Fig. 15: Driving signal generation circuit

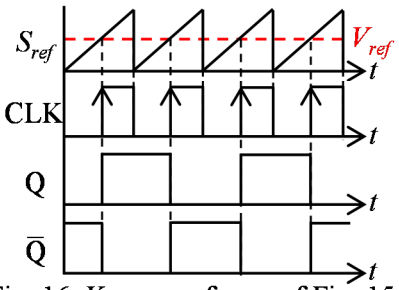

Fig. 16: Key waveforms of Fig. 15

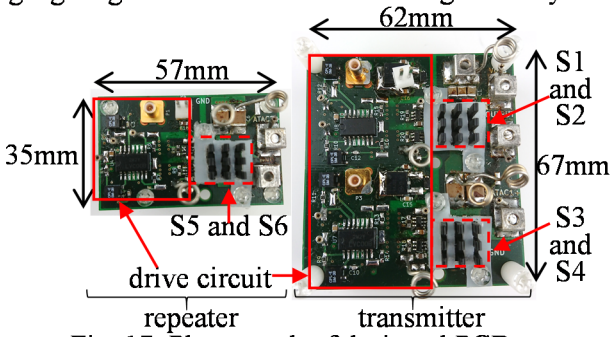

Fig. 17: Photograph of designed PCB

generator and the external power supply is out of the scope of this paper. The self-drive technique will be presented in another paper.

However, as a first step to achieve the self-drive technique, this paper presents a circuit to generate the driving signals for all the switches of Fig. 14 by using only a single reference signal, which is an elemental technique to realize the self-drive. As mentioned in the previous section, the half-bridge inverter and the ATACs must operate with the different phase in synchronization. Figure 15 shows the driving signal generation circuit. Then, Fig. 16 shows the key waveforms of Fig. 15. In Fig. 16, the sawtooth wave of S_{ref} is the reference signal generated by using the signal generator. The frequency of S_{ref} is 13.56 MHz. Then, S_{ref} and DC voltage of V_{ref} are compared by the comparator. The output terminal of the comparator is connected to the CLK terminal of the D-flip flop (D-FF). The D terminal and $\overline{Q}$ terminal of the D-FF are short-circuited. As a result, the square waves of 6.78 MHz with 50% duty cycle can be obtained. Then, the driving signals can be generated via the dead time generation circuit. The level of V_{ref} can control the phase difference between the driving signals and S_{ref}. Finally, Fig. 17 shows the photograph of the designed PCB.

Experimental Setup and Experimental Method

Then, this subsection describes the experimental setup and the experimental method. Table I shows the circuit parameters for the experiments. In this paper, the resonators are designed to be resonant at 6.78 MHz. Figure 18 shows the photograph of the experimental setup.

Table I. Circuit Parameters

Input DC voltage	V_{DC}	14 V
Self-inductance of W_1	L_1	2.45 μH
Parasitic resistance of W_1	r_1	0.663 Ω
Capacitance of transmitter	C_1	228 pF
Self-inductance of W_2	L_2	2.35 μH
Parasitic resistance of W_2	r_2	0.645 Ω
Capacitance of repeater	C_2	231 pF
Self-inductance of W_3	L_3	0.653 μH
Parasitic resistance of W_3	r_3	0.182 Ω
Capacitance of receiver	C_3	841 pF
Load resistance	R_L	30 Ω
Operating frequency	f_S	6.78 MHz

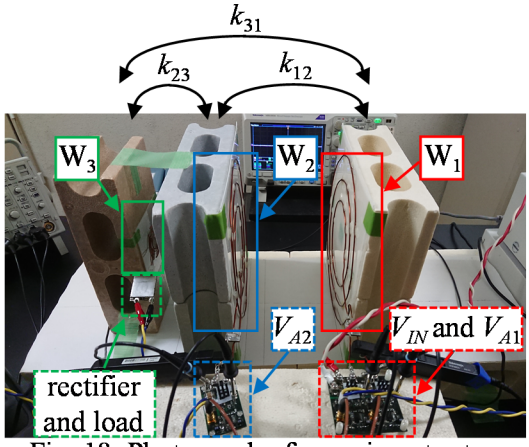

Fig. 18: Photograph of experiment setup

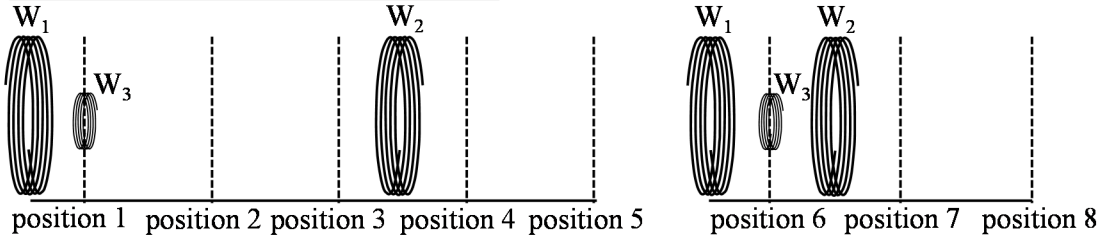

(a)k_{12}=0.0293 (b)k_{12}=0.0693

Fig. 19: Position of receiver

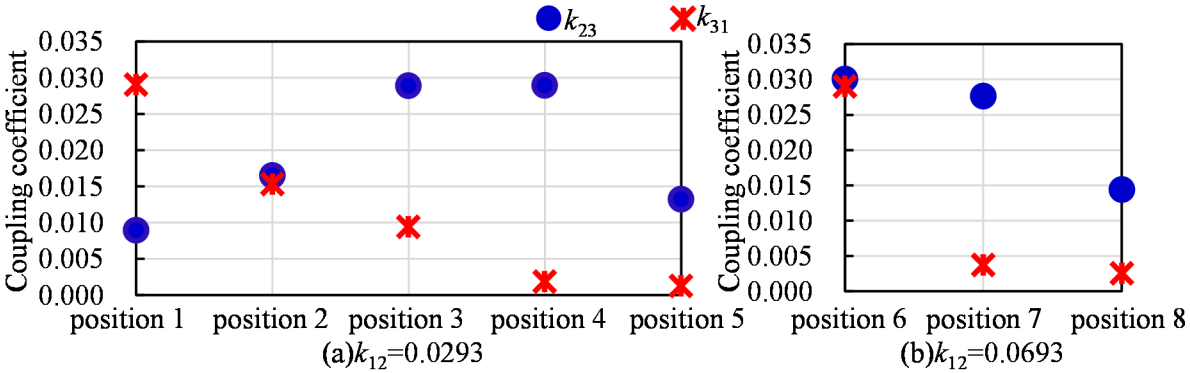

(a)k_{12}=0.0293 (b)k_{12}=0.0693

Fig. 20: Coupling coefficient at all positions

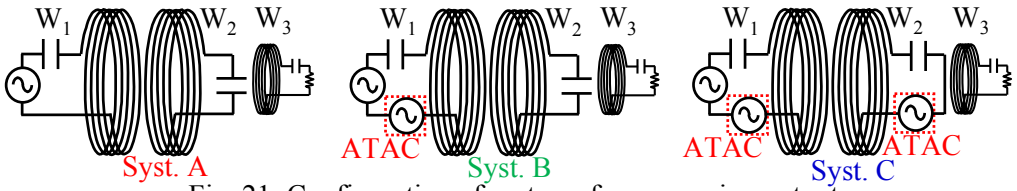

Fig. 21: Configuration of systems for comparing output power

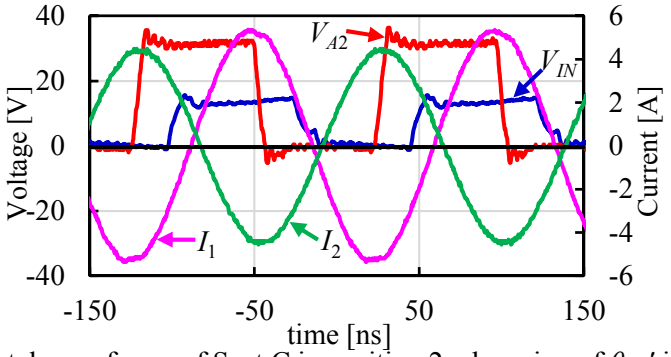

Fig. 22: Experimental waveforms of Syst.C in position 2 when sign of θ_{opt}' is set to positive

In the experiments, we measure the output power of the receiver at eight positions as shown in Fig. 19. There are two types of positions of the repeater (k_{12}=0.0293 and k_{12}=0.0693), which satisfy the condition of Re[Z_{12}]>r_1+Re[Z_{31}]. Figure 20 shows the coupling coefficient (k_{23} and k_{31}) at position 1–position 8. To verify the effectiveness of the impedance matching method using the ATACs, we compare the output powers of the three systems as shown in Fig. 21. In Fig. 21, System A is the RIC-WPT without the ATACs; System B is the RIC-WPT with the ATAC on only the transmitting side; System C is the RIC-WPT with the ATACs.

Then, we determine the sign of θ_{opt}' for the measurement of the output power of system C. In this experiment, to obtain a high output power at the center between the transmitter and the repeater, the sign of θ_{opt}' is set to positive. Figure 22 shows the experimental waveforms in position 2 when the sign of θ_{opt}' is set to positive. In the experiment, θ_{opt}' is defined as θ where measured I_2 is maximized. As shown in Fig. 22, the phases of I_1 and I_2 are close to the opposite phase. As pointed out in [11], at this condition, the magnetic field at the center between the transmitter and the repeater is stronger than that when the phases of I_1 and I_2 are close to the same phase. As shown in Fig. 22, the relation between V_{IN} and I_1 is set to slightly inductive so that the S1 and S2 achieve zero-voltage-switching (ZVS).

Experimental results

Finally, this subsection compares the output power between the three systems. Figure 23 shows the comparison results of the output power. Furthermore, Fig. 24 shows the frequency characteristics of the output power in the positions 1, 2, 4, and 7. From Fig. 23, system C achieves the higher output power than the other systems in all positions. As shown in Fig. 24, systems A and B is difficult to obtain a large power due to the frequency splitting phenomenon. Furthermore, the frequencies corresponding to the

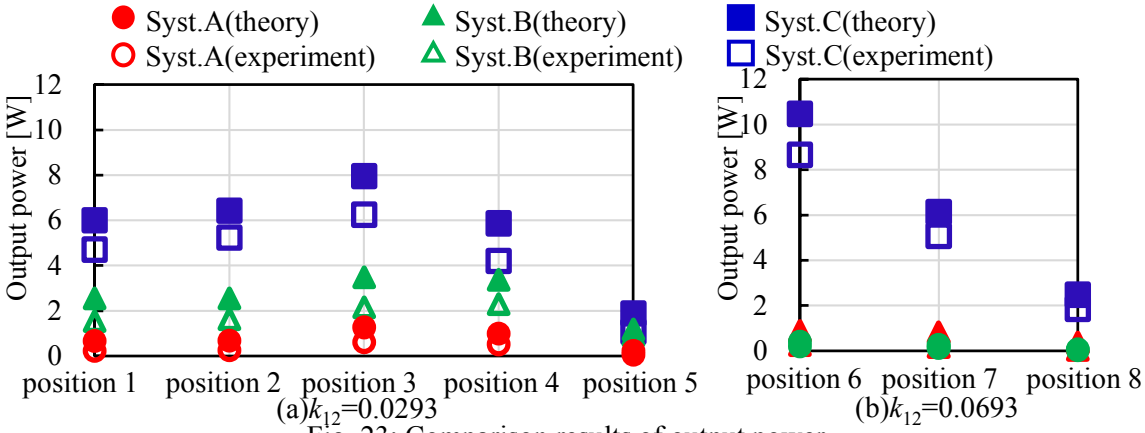

(a)k_{12}=0.0293 (b)k_{12}=0.0693

Fig. 23: Comparison results of output power

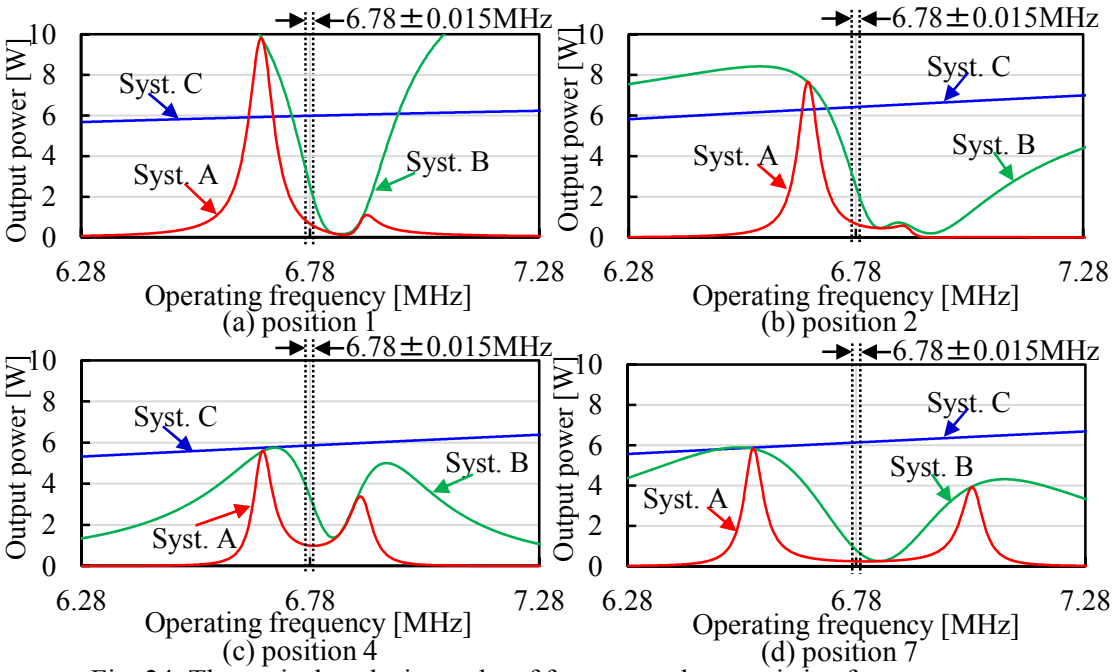

Fig. 24. Theoretical analysis results of frequency characteristic of output power

peaks dramatically change according to the positions of the repeater. Therefore, systems A and B requires the accurate adjustment of the resonant frequencies of the resonator based on the position of the repeater. On the other hand, the frequency characteristic of the output power of system C is not affected by the frequency splitting phenomenon, which means that the repeater current of system C is constant regardless of the position of the repeater. This advantage allows system C to obtain the high output power at positions 5 and 8.

Although system C shows the attractive characteristic, there are slight errors between the experimental results and the theoretical analysis results in all positions. The error occurs because the slight error of the ATACs equivalently reduces the *Q*-factor of the resonators. From the experimental results, the total loss of the ATACs in all position can be roughly estimated. As a result, the average loss of the ATAC on the transmitting side is 0.8W. Furthermore, the average loss of the ATAC on the repeating side is 1.18W. Despite these slight losses, system C achieves large output power in a wider space compared to systems A and B. From the above results, the effectiveness of the impedance matching method using the ATAC for improving the spatial freedom of 6.78 MHz RIC-WPT can be verified.

Conclusion

To increase the spatial freedom of the 6.78 MHz RIC-WPT by using the repeater is practically difficult due to the frequency splitting phenomenon. To maintain the output power even when the frequency splitting phenomenon occurs, we must readjust the resonant frequency of the resonators according to the position of the repeater.

To address this difficulty, we applied the impedance matching method using the ATACs to the 6.78MHz RIC-WPT. First, in this paper, we revealed that the impedance matching method using the ATACs could maximize the repeater current even in the system including the receiver. Then, we carried out the experiments to verify the effectiveness of the impedance matching method using the ATACs. The experimental results showed that the system with ATACs could improve the output power at the receiver in a wide range regardless of the frequency splitting phenomenon. This suggests that the impedance matching method using ATACs is promising to increase the spatial freedom of the 6.78 MHz RIC-WPT system with the repeater.

References

[1] J. Kim, H.-C. Son, D.-H. Kim, and Y.-J. Park, “Optimal design of a wireless power transfer system with multiple self-resonators for an LED TV,” IEEE Trans. Consum. Electron., vol. 58, no. 3, pp. 775–780, Aug. 2012.

[2] N. S. Jeong and F. Carobolante, “Wireless charging of a metal-body device,” IEEE Trans. Microw. Theory Techn, vol. 65, no. 4, pp. 1077–1086, Apr. 2017.

[3] S. A. Mirbozorgi, Y. Jia, D. Canales, and M. Ghovanloo, “A wirelessly-powered homecage with segmented copper foils and closed-loop power control,” IEEE Trans. Biomed. Circuits Syst., vol. 10, no. 5, pp. 979–989, Oct. 2016.

[4] S. Mao, J. Zhang, K. Song, G. Wei, and C. Zhu, “Wireless power transfer using a field-enhancing coil and a small-sized receiver with low coupling coefficient,” IET power electron., vol. 9, no. 7, pp. 1546–1552, Jun. 2016.

[5] M. Fu, H. Yin, M. Liu, Y. Wang, and C. Ma, “A 6.78 MHz multiple-receiver wireless power transfer system with constant output voltage and optimum efficiency,” IEEE Trans. Power Electron., vol. 33, no. 6, pp. 5330–5340, Jun. 2018.

[6] E. Ozalevli, N. Femia, G. D. Capua, R. Subramonian, D. Du, J. Sankman, and M. E. Markhi, “A cost-effective adaptive rectifier for low power loosely coupled wireless power transfer systems,” IEEE Trans. Circuits Syst. I, Reg. Papers, vol. 65, no. 7, pp. 2318–2329, Jul. 2018.

[7] H.-G. Park, J.-H. Jang, H.-J. Kim, Y.-J. Park, S. Oh, Y. Pu, K. C. Hwang, Y. Yang, and K.-Y. Lee, “Design of a wireless power receiving unit with a high-efficiency 6.78-MHz active rectifier using shared DLLs for magnetic-resonant A4WP applications,” IEEE Trans. Power Electron., vol. 31, no. 6, pp. 4484–4498, Jun. 2016.

[8] W. X. Zhong, C. Zhang, X. Liu, and S. Y. R. Hui, “A methodology for making a three-coil wireless power transfer system more energy efficient than a two-coil counterpart for extended transfer distance,” IEEE Trans. Power Electron., vol. 30, no. 2, pp. 933–942, Feb. 2015.

[9] K. Lee and S. H. Chae, “Power transfer efficiency analysis of intermediate-resonator for wireless power transfer,” IEEE Trans. Power Electron., vol. 33, no. 3, pp. 2484–2493, Mar. 2018.

[10] D. Ahn and S. Hong, “A study on magnetic field repeater in wireless power transfer,” IEEE Trans. Ind. Electron., vol. 60, no. 1, pp. 360–371, Jan. 2013.

[11] R. Huang, B. Zhang, D. Qiu, and Y. Zhang, “Frequency splitting phenomena of magnetic resonant coupling wireless power transfer,” IEEE Trans. Magn., vol. 50, no. 11, 8600204, Nov. 2014.

[12] W.-Q. Niu, J.-X. Chu, W. Gu, and A.-D. Shen, “Exact analysis of frequency splitting phenomena of contactless power transfer systems,” IEEE Trans. Circuits Syst. I, Reg. Papers, vol. 60, no. 6, pp. 1670–1677, Jun. 2013.

[13] Y. -L. Lyu, F. -Y. Meng, G. -H. Yang, B. -J. Che, Q. Wu, L. Sun, D. Erni, and J. L. -W. Li, “A method of using nonidentical resonant coils for frequency splitting elimination in wireless power transfer,” IEEE Trans. Power Electron., vol. 30, no. 11, pp. 6097–6107, Nov. 2015.

[14] M. Ishihara, K. Umetani, and E. Hiraki, “Impedance matching to maximize induced current in repeater of resonant inductive coupling wireless power transfer systems,” in Proc. IEEE Energy Convers. Congr. Expo., Portland, USA, Sep. 2018, pp. 6194–6201.

[15] Y. Endo and Y. Furukawa, “Proposal for a new resonance adjustment method in magnetically coupled resonance type wireless power transmission,” in Proc. 2012 IEEE MTT-S Int. Microw. Workshop Series on Innovative Wireless Power Transmission: Tech., Syst., and Appl. (IMWS-IWPT), 2012, pp. 263–266.

[16] B. Esteban, M. Sid-Ahmed, and N. C. Kar, “A comparative study of power supply architectures in wireless EV charging systems,” IEEE Trans. Power Electron., vol. 30, no. 11, pp. 6408–6422, Nov. 2015.

[17] K. Song, Z. Li, J. Jiang, and C. Zhu, “Constant current/voltage charging operation for series–series and series–parallel compensated wireless power transfer systems employing primary-side controller,” IEEE Trans. Power Electron., vol. 33, no. 9, pp. 8065–8080, Sep. 2018.

[18] K. Umetani, R. Matsumoto, and E. Hiraki “Prevention of oscillatory false triggering of GaN-FETs by balancing gate-drain capacitance and common-source inductance,” IEEE Trans. Ind. Appl., vol. 55, no. 1, pp. 610–619, Jan./Feb. 2019.

[19] D. Reusch, and J. Strydom, “Understanding the effect of PCB layout on circuit performance in a high-frequency gallium-nitride-based point of load converter,” IEEE Trans. Power Electron., vol. 29, no. 4, pp. 2008–2015, Apl. 2014.